Supporting Information

Benzimidazole-linked Bimetallic Phthalocyanine-Porphyrin Covalent Organic Framework Synergistically Promotes CO_2 Electroreduction

Xiao-Yu Dong, Fang-Qin Yan, Qian-You Wang, Peng-Fei Feng, Ru-Yi Zou, Shan Wang* & Shuang-Quan Zang**

Henan Key Laboratory of Crystalline Molecular Functional Materials, Green Catalysis Center, and College of Chemistry, Zhengzhou University, Zhengzhou 450001, China.

E-mail: zangsqzg@zzu.edu.cn, shanwang@zzu.edu.cn, ryzou@zzu.edu.cn

Experimental Procedures

1.Methods and Materials

Characterization.

^{1}H-NMR and ^{13}C NMR spectra were measured on Bruker AVIII HD 600 instrument. Powder X-ray diffraction (PXRD) patterns of the samples were recorded on a D/MAX-3D diffractometer by depositing powder on glass substrate, from 2θ = 3° up to 50° with 0.02° increment. Fourier transform infrared (FT-IR) spectra were recorded on a Bruker ALPHA II FT-IR spectrometer. The X-ray photoelectron spectroscopy (XPS) data were collected using ESCALAB 250 system (Thermo Electron). The C peak at 284.8 eV was used as a reference to correct for charging effects. Field-emission scanning electron microscopy (FESEM) measurement was carried out using Zeiss Sigma 500. Transmission electron microscopy (TEM) images were obtained in FEI TalosF200S. Aberration-corrected HAADF-STEM (AC HAADF-STEM) images were obtained in FEI Titan cubed Themis G2 300 STEM with aspherical aberration corrector. Element analyses (EA) were collected on a PerkinElmer 240 elemental analyzer. The inductively coupled plasma mass Optical Emission Spectrometer (ICP-OES) spectroscopy analysis was recorded on Optimass 9500. Thermal gravimetric analysis (TGA) was recorded by TGA Q50 thermal analyzer from room temperature to 800 ^{o}C under N_2 atmosphere using a heating rate of 10 ^{o}C min^{-1}. N_2 adsorption isotherms were measured at liquid nitrogen temperature (77 K) by using automatic volumetric adsorption equipment (Belsorp Max) after a degassed process at 120 ^{o}C for 12 h. Specific surface areas were obtained by using the Brunauer-Emmet-Teller (BET) model. By using the nonlocal density functional theory (NLDFT) model, the pore volume was derived from the sorption curve. CO_2 adsorption isotherms were measured at 298 K by using automatic volumetric adsorption equipment (Belsorp Max) after a degassed process at 120 ^{o}C for 12 h. Electrochemical test was carried out on electrochemical working station CHI 660E (Shanghai). The produced gas was monitored by Agilent GC7820 Gas Chromatograph (N_2 as gas carrier, and the columns of GC are Porapak Q and MolSieve 5A). The HRESI-TOF-MS spectra was collected on an AB Sciex X500R Q-TOF spectrometer. Isotopic labeling control experiments were obtained on gas chromatography-mass spectrometry (7890A and 5975C, Agilent

Technologies). The electronic measurement was realized by a semiconductor analyzer (B1500A, Keysight), and the electrode device is in a probe station (CGO-4, Cindbest).

Chemicals.

Unless otherwise specified, all chemicals were obtained from commercial source without additional drying or degassing. Tetra (4-aldehyde phenyl) porphyrin was purchased from commercial purchase, 2,3,9,10,16,17,23,24-octa-aminophthalocyanine nickel ($8NH_2$-NiPc) and 5,10,15,20-tetrakis(4-formylphenyl)porphyrin cobalt (4CHO-CoPor) were referred to in the literature.[1,2]

Computational Calculation.

All the calculations were performed within the framework of the density functional theory (DFT) as implemented in the Vienna Ab initio Software Package (VASP 5.3.5) code within the Perdew–Burke–Ernzerhof (PBE) generalized gradient approximation and the projected augmented wave (PAW) method.[3-6] The cutoff energy for the plane-wave basis set was set to 400 eV. The Brillouin zone of the surface unit cell was sampled by Monkhorst–Pack (MP) grids, with k-point mesh for NiPc-MPOP surface optimizations.[7] The NiPc-MPOP surface was determined by 2 × 2 × 1 Monkhorst−Pack grid. The convergence criterion for the electronic self-consistent iteration and force was set to 10^{-7} eV and 0.01 eV/Å, respectively. A vacuum layer of 12 Å was introduced to avoid interactions between periodic images.

The free energies of adsorbates at temperature T were estimated according to the harmonic approximation, and the entropy is evaluated using the following equation:

$$S(T) = K_B + \sum_{i}^{harm\ DOF} \left(\frac{\varepsilon_i}{K_B T (e^{\frac{\varepsilon_i}{K_B T}} - 1)} - ln(1 - e^{-\frac{\varepsilon_i}{K_B T}}) \right)$$

where K_B is Boltzmann's constant and DOF is the number of harmonic energies (ε_i) used in the summation denoted as the degree of freedom, which is generally 3N, where N is the number of atoms in the adsorbates. Meanwhile, the free energies of gas phase species are corrected as:

$$G_g(T) = E_{elec} + E_{ZPE} + \int C_p dT - TS(T)$$

where C_p is the gas phase heat capacity as a function of temperature derived from Shomate equations and the corresponding parameters in the equations were obtained from NIST.

Synthesis of Model Compound.

1,4-bis(1H-benzo[d]imidazol-2-yl)benzene (**M1**) was synthesized by the condensation reaction between terephthalaldehyde (BDA) and *o*-Phenylenediamine (OPD) (Scheme S1). A mixture of 40 mg (0.30 mmol) BDA and 105 mg (0.97 mmol) OPD in 5 mL EtOH/dioxane (4:1) mixture and 0.15 mL AcOH (6 M) were sealed in a 10 mL pressure-resistant tube, heated at 100 °C for 24 h and then cooled to room temperature. A pale yellow solid was obtained by filtration, washed with copious amount of EtOH and air dried. ^{1}H NMR (600 MHz, DMSO-d_6): δ 7.26 (m, 4H), 7.70 (m, 4H), 8.36 (s, 4H), 13.04 (s, 2H) (Fig. S1). MALDI-TOF MS: m/z calculated for $C_{20}H14N4$ $[M]^-$: 310.132, measured: 310.132 (Fig. S2).

Synthesis of NiPc-CoPor-imi-COF.

8NH_2-NiPc (10 mg, 0.014 mmol) and 4CHO-CoPor (12 mg, 0.015 mmol) were mixed in the solvent of DMAc and Mesitylene (1 mL, 1:4, v/v) in a Penicillin vial. The resulting mixture was sonicated for three minutes, aqueous acetic acid (6.0 M, 0.2 mL) was added. Then heated at 150 °C in an isothermal oven for 3 days. The precipitate was collected via centrifugation, washed three times with DMAc. To remove the trapped guest molecules, NiPc-CoPor-imi-COF was subjected to Soxhlet extraction with THF for 1 day. And the dark green powder was collected after drying at 120 °C under vacuum overnight.(Scheme S2)

Synthesis of CoPor-imi-COP.

The synthetic conditions of CoPor-imi-COP were similar to that of NiPc-CoPor-imi-COF. BTA (12 mg, 0.042 mmol) and 4CHO-CoPor (15 mg, 0.019 mmol) were mixed in the solvent of DMAc and Mesitylene (2 mL, 3:1, v/v), aqueous acetic acid (6.0 M, 0.1 mL) was added, then heated at 120 ^{o}C for 3 days. Dark purple precipitates were produced and isolated through centrifugation, washed with DMAc and THF, finally drying in a vacuum dryer (Scheme S3).

Synthesis of NiPc-imi-COF.

8NH_2-NiPc (20 mg, 0.028 mmol) and BDA (8 mg, 0.060 mmol) were mixed in the solvent of DMAc and Mesitylene (1.4 mL, 4:3, v/v) in a Penicillin vial. Acetic-acid (0.1 mL) was added. Then heated at 150 ^{o}C for 3 days. Dark green precipitates were produced and isolated through centrifugation, washed with DMAc and THF, finally drying in a vacuum dryer (Scheme S4).

Electrode Preparation.

3 mg of COFs and 1.5 mg of Ketjen black were ground for 3 min, then ethanol (300 μL) and Nafion perfluororesin solution (20 μL, 5 wt%) were added, and a paste was obtained after sonication for 30 min. The paste was drop-coated on hydrophilic carbon paper (1×1 cm^2) to prepare COF composites with a loading density of 1 mg cm^{-2}. Dry the composite paper at room temperature for 3 hours. The control experiments with other materials as working electrodes were conducted under similar conditions.

Electrochemical Measurements.

The CO_2RR performance was measured in CO_2-saturated 0.5 M $KHCO_3$ aqueous solutions (pH = 7.2) using a gas-tight H-type electrochemical cell (separated by proton exchange membrane), and the working electrode and counter electrode are separated in different compartments. The counter electrode and reference electrode are platinum net and Ag/AgCl electrode, respectively. All mentioned potentials were converted to a RHE scale according to the equation of E (V vs. RHE) = E (vs. Ag/AgCl) + 0.059 × pH + 0.197. CO_2 gas was delivered at an average rate of 25 mL min^{-1} (at room temperature and ambient pressure), and the produced gas was analyzed by GC every 30 min. The separated gas products were

analyzed by Agilent GC7820 Gas Chromatograph. The liquid products were analyzed afterwards by quantitative NMR (Bruker AVIII HD 600).

The separated gas products were analyzed by Agilent GC7820 Gas Chromatograph. The liquid products were analyzed afterwards by quantitative NMR (Bruker AVIII HD 600).

Faradic efficiency calculation for CO (FE_{CO}):

$$FE_{CO} = \frac{Q_{CO}}{Q_{total}} = \frac{n_{CO} \times N \times F}{Q_{total}}$$

Q_{CO}: the amount of charge required to generate the product;

Q_{total}: the total amount of charge transferred during the catalytic process;

n_{CO}: the production of CO (measured by GC), mol;

N: the number of electron transferred for product formation, in which it is 2 for CO;

F: Faradaic constant, 96485 C mol^{-1}.

The turnover frequency (TOF, s^{-1}) values are calculated based on the ICP results of COFs.

$$TOF_{ICP} = \frac{FE_{CO} \times j_{total}}{N \times F \times \frac{\omega \times m}{M_{metal}}}$$

FE_{CO}: Faraday efficiency of CO;

j_{total}: total current, A;

N: the number of electron transferred for product formation, in which it is 2 for CO;

F: Faradaic constant, 96485 C mol^{-1};

m: catalyst mass in the electrode, g;

ω: metal loading in the catalyst;

M_{metal}: atomic mass of metal.

Measurements of Conductivity.

Electrical measurement of the materials was performed using two-electrode in air at a constant temperature of 298 K in the absence of light. And in order to prepare a pressed pellet, samples was added to a sleeve pressing die and pressed. After trimming, the length of the device was 3mm, width was 1.5mm,

and thickness was 0.1mm. Current-voltage (I-V) curves were registered in the voltage range of −1.0 ~ +1.0 V. Conductivity (σ) was obtained by the following equation: $\sigma = \frac{LI}{U \times S}$

L: the overlapping length of the electrodes, m;

I: the current, A;

U: the potential, V;

S: the cross sectional area of electrode, m^{-2}.

2. Supporting Figs.

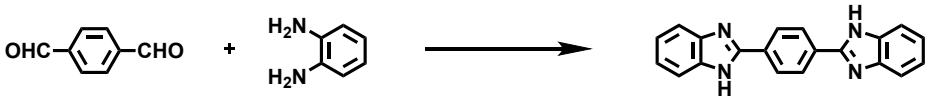

Scheme S1. Synthesis of **M1**.

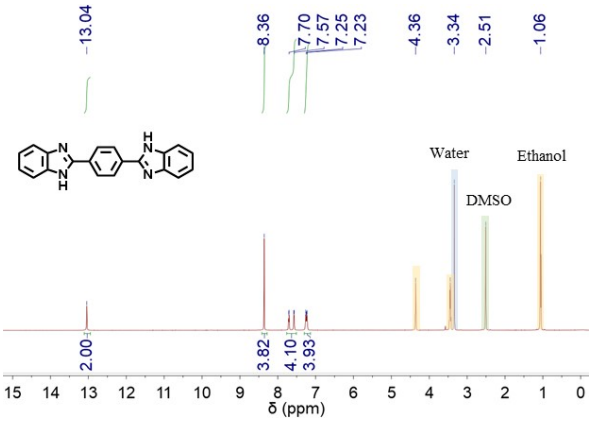

Fig. S1. ^{1}H NMR spectra of **M1**.

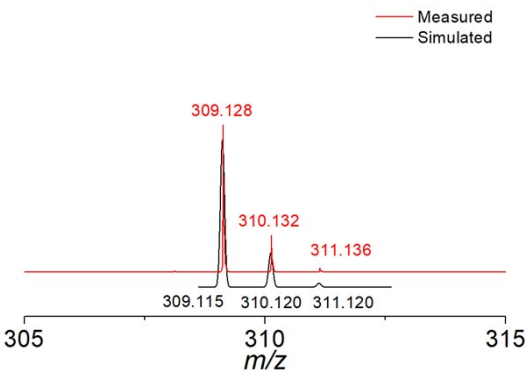

Fig. S2. The negative-ion mode ESI-TOF-MS spectra of **M1**.

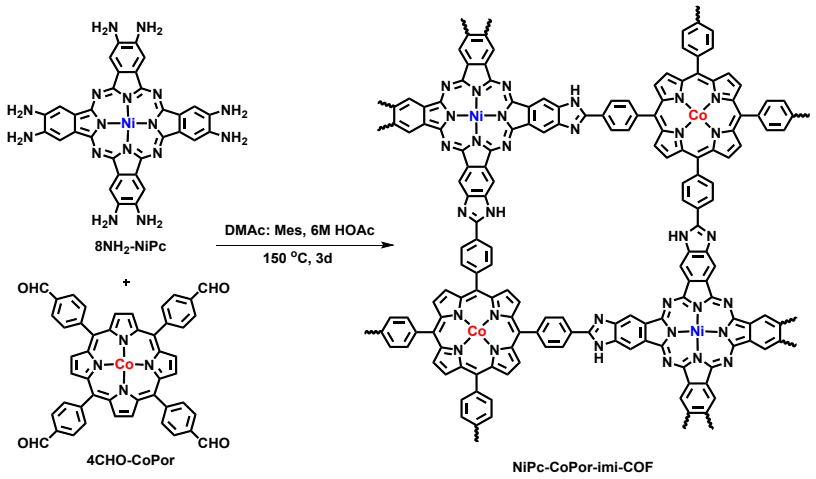

Scheme S2. Synthesis of **NiPc-CoPor-imi-COF**.

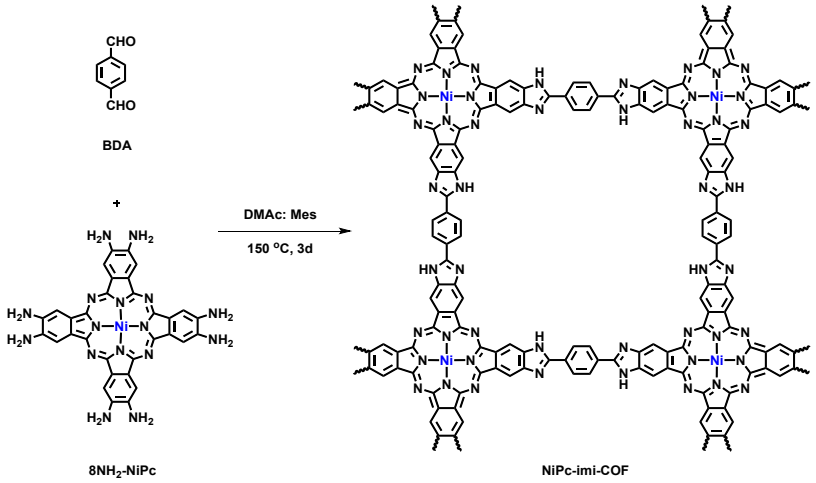

Scheme S3. Synthesis of **NiPc-imi-COF**.

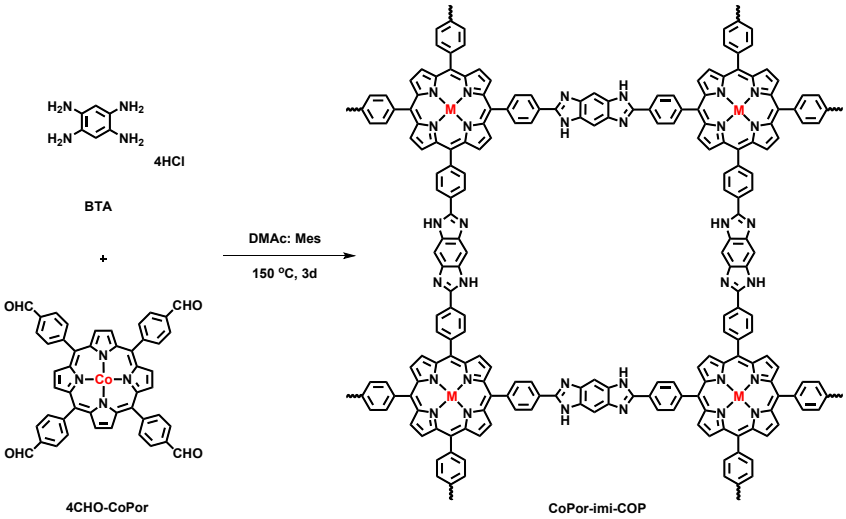

Scheme S4. Synthesis of **CoPor-imi-COP**.

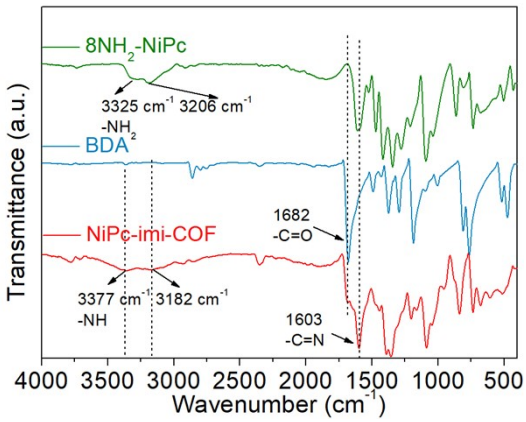

Fig. S3. FT-IR spectra of NiPc, BDA, and NiPc-imi-COF.

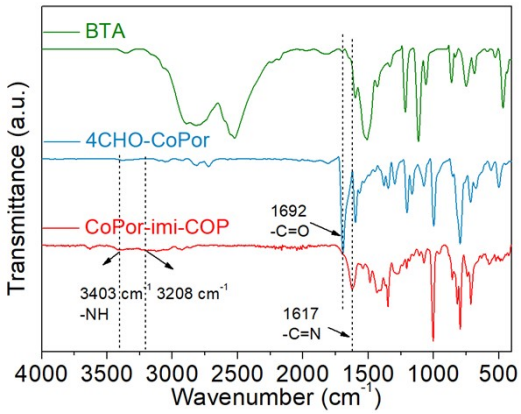

Fig. S4. FT-IR spectra of BTA, CoPor, and CoPor-imi-COP.

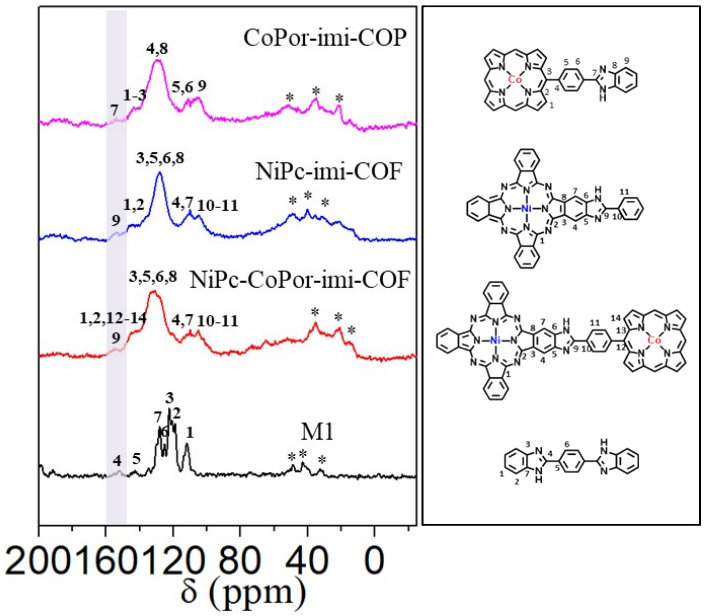

Fig. S5. ^{13}C solid-state NMR spectra of M1, NiPc-CoPor-imi-COF, NiPc-imi-COF, and CoPor-imi-COP.

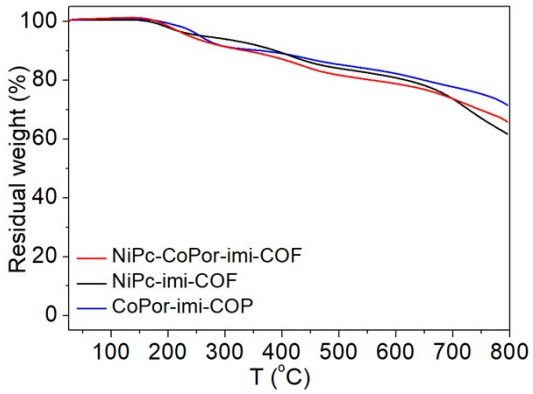

Fig. S6. TGA spectra of NiPc-CoPor-imi-COF, NiPc-imi-COF, and CoPor-imi-COP.

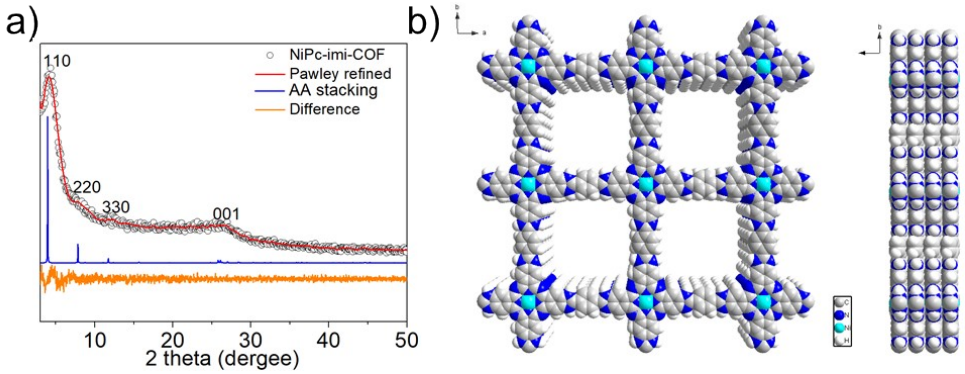

Fig. S7. a) Overlay of the experimental and calculated PXRD traces obtained for NiPc-imi-COF. Pawley refinement was applied to obtain the converged unit cell parameters. b) Top view of simulated AA stacking mode and side view of AA stacking mode for NiPc-imi-COF crystal structure.

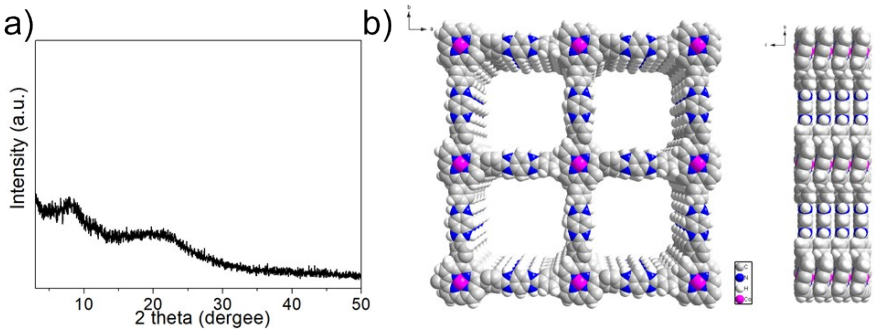

Fig. S8. a) PXRD of CoPor-imi-COP. b) Top view of simulated AA stacking mode and side view of AA stacking mode for CoPor-imi-COP crystal structure.

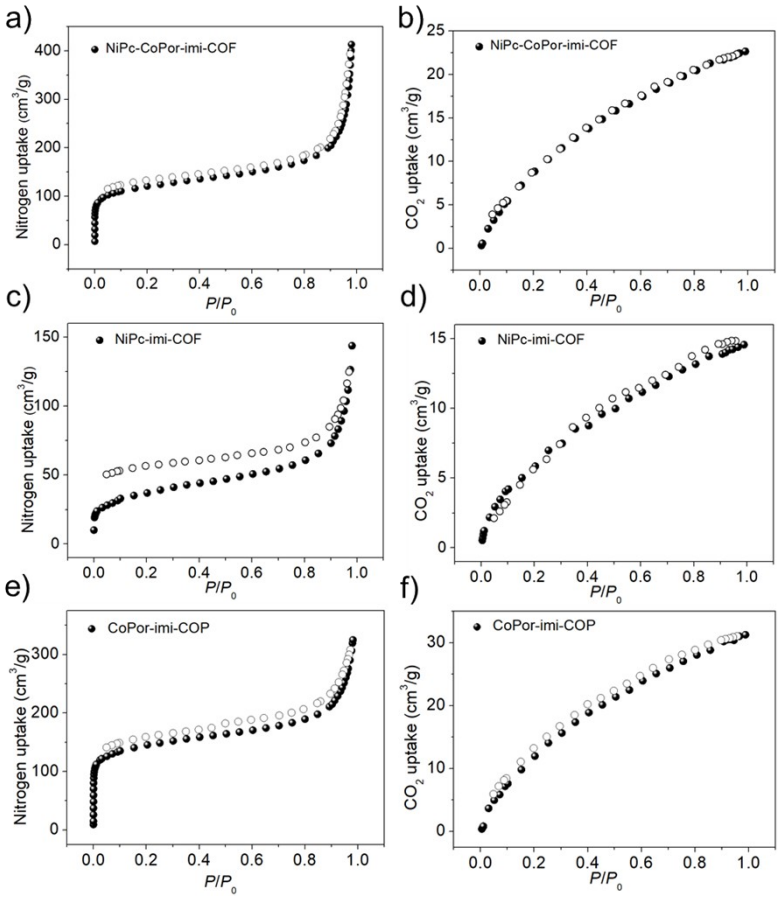

Fig. S9. N_2 sorption isotherm of a) NiPc-CoPor-imi-COF, c) NiPc-imi-COF, and e) CoPor-imi-COP. CO_2 sorption isotherms of b) NiPc-CoPor-imi-COF, d) NiPc-imi-COF, and f) CoPor-imi-COP measured at 298 K.

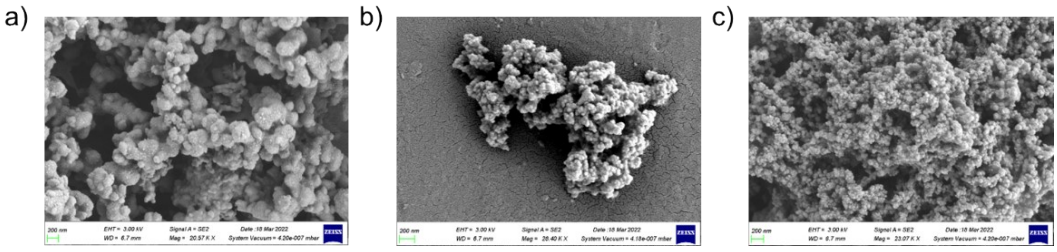

Fig. S10. FE-SEM images of a) NiPc-CoPor-imi-COF, b) NiPc-imi-COF, and c) CoPor-imi-COP.

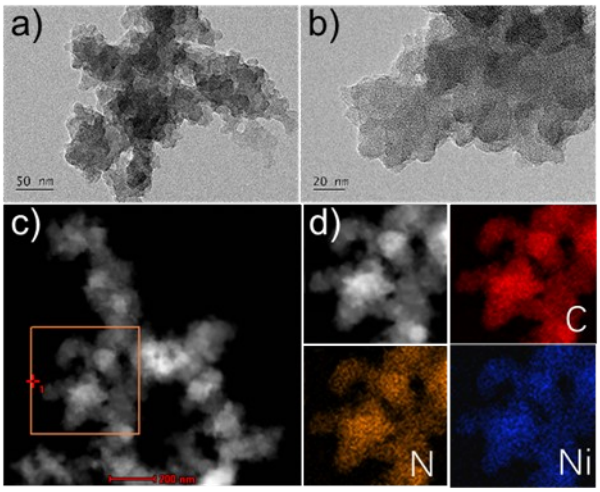

Fig. S11. a) and b) TEM of NiPc-imi-COF. c) and d) EDS analysis results of NiPc-imi-COF

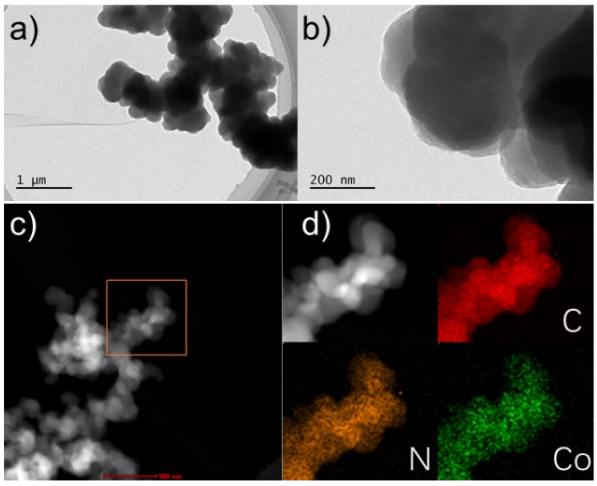

Fig. S12. a) and b) TEM of CoPor-imi-COP. c) and d) EDS analysis results of CoPor-imi-COP.

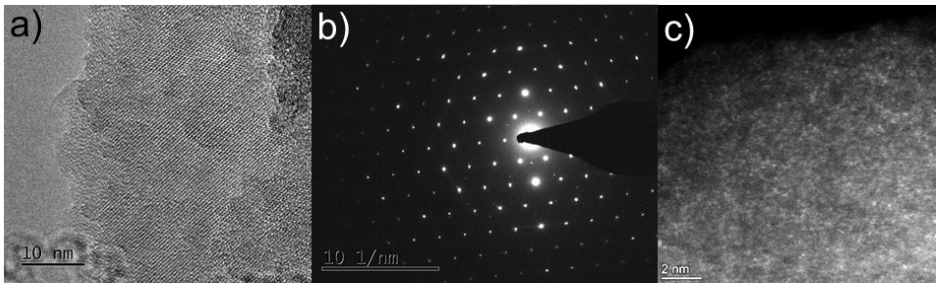

Fig. S13. a) HRTEM, b) SAED, and b) HAADF-STEM images of NiPc-CoPor-imi-COF.

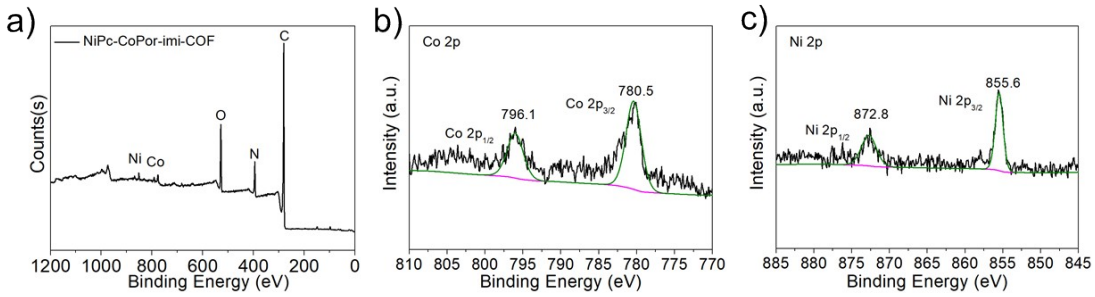

Fig. S14. XPS spectra of NiPc-CoPor-imi-COF. a) Total XPS spectra. b) Co 2p. c) Ni 2p.

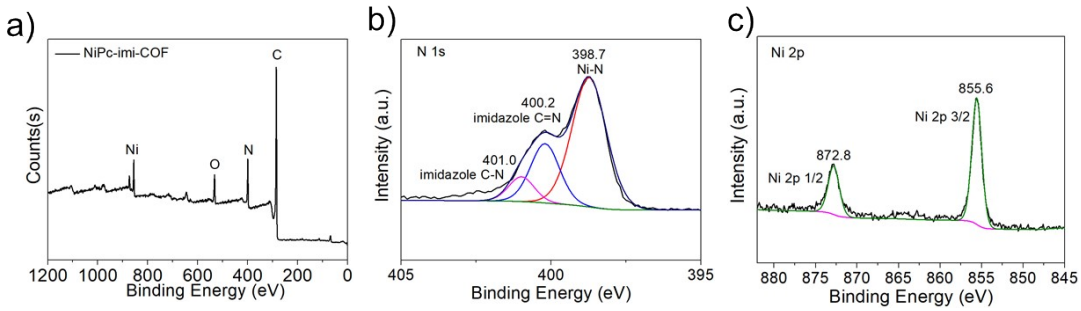

Fig. S15. XPS spectra of NiPc-imi-COF. a) Total XPS spectra. b) N1s. c) Ni 2p.

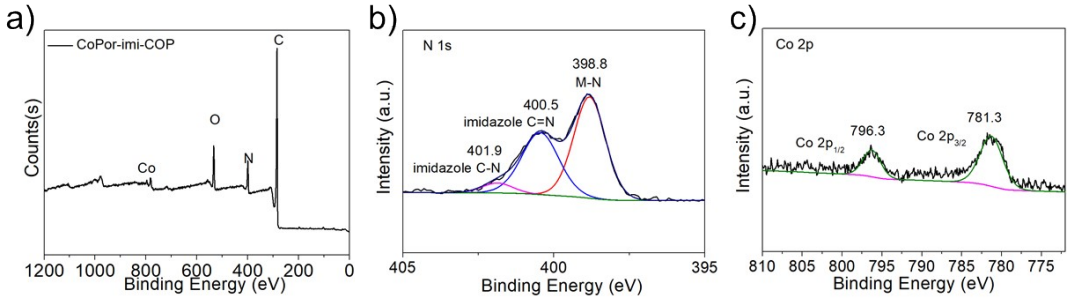

Fig. S16. XPS spectra of CoPor-imi-COP. a) Total XPS spectra. b) N1s. c) Co 2p.

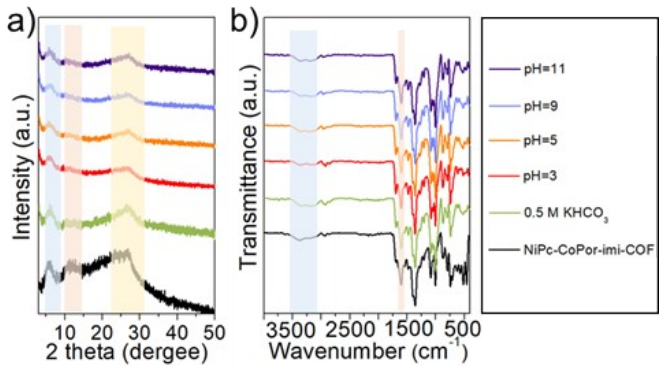

Fig. S17. PXRD patterns a) and IR b) measured after 3-days treatment of NiPc-CoPor-imi-COF in aqueous KOH (pH=9, 11), HCl (pH=3, 5) and 0.5 M $KHCO_3$.

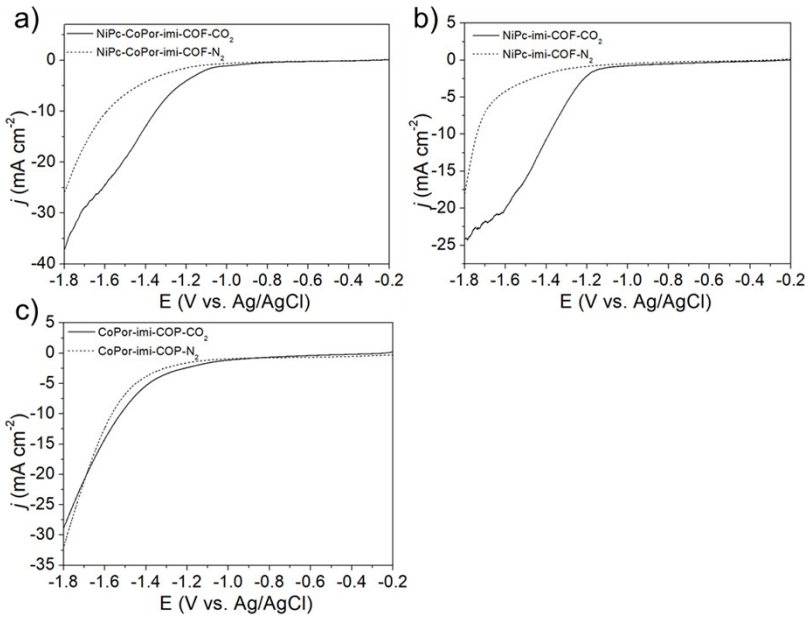

Fig. S18. LSV curves for COFs in a CO_2-saturated and N_2-saturated $KHCO_3$ solution at the potential range of −1.8 to −0.2 V (vs Ag/AgCl, scan rate of 10 mV/s).

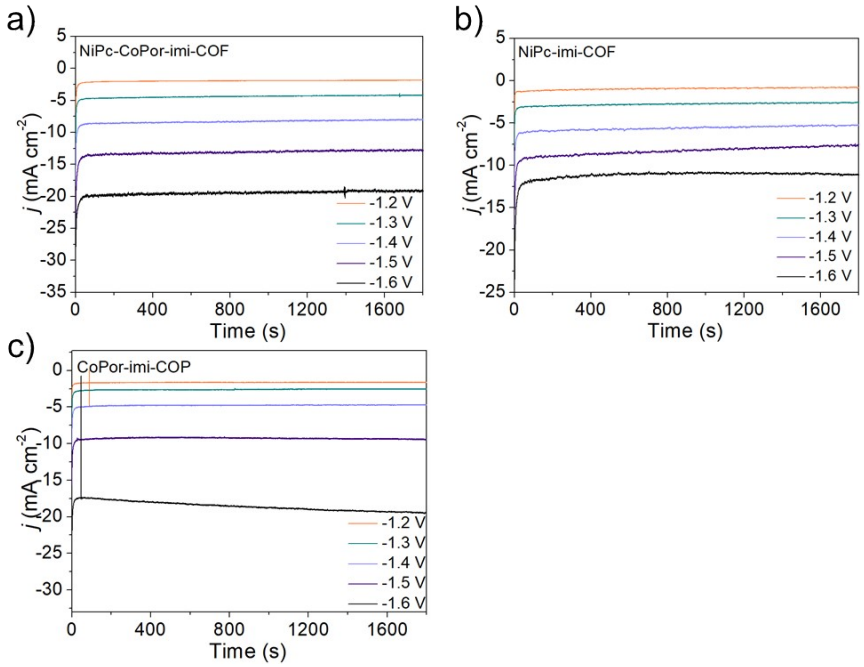

Fig. S19. Chronoamperometric responses of COFs at different potentials (−1.2 to −1.6 V, vs Ag/AgCl)

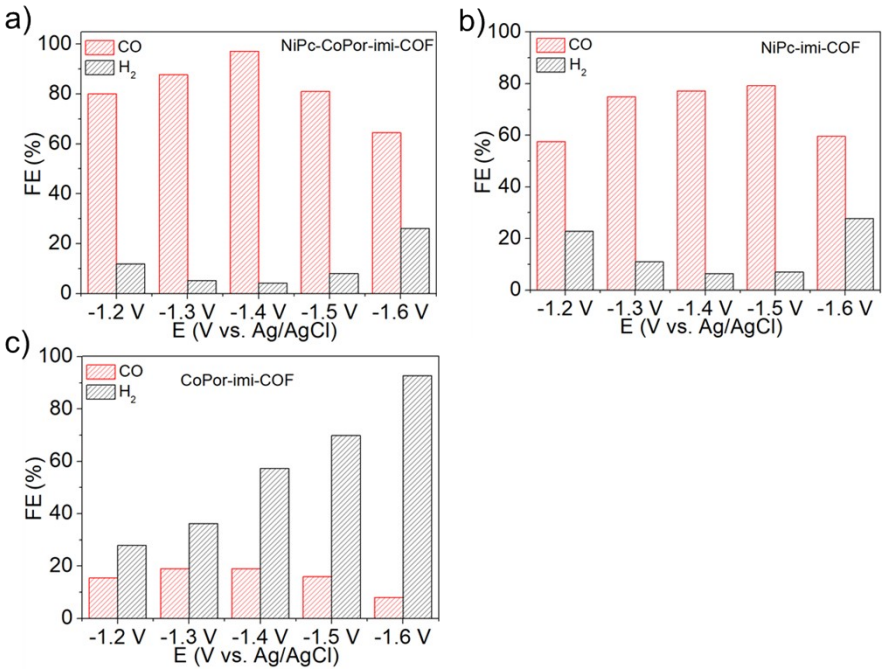

Fig. S20. FE of NiPc-CoPor-imi-COF , NiPc-imi-COF, and CoPor-imi-COP.

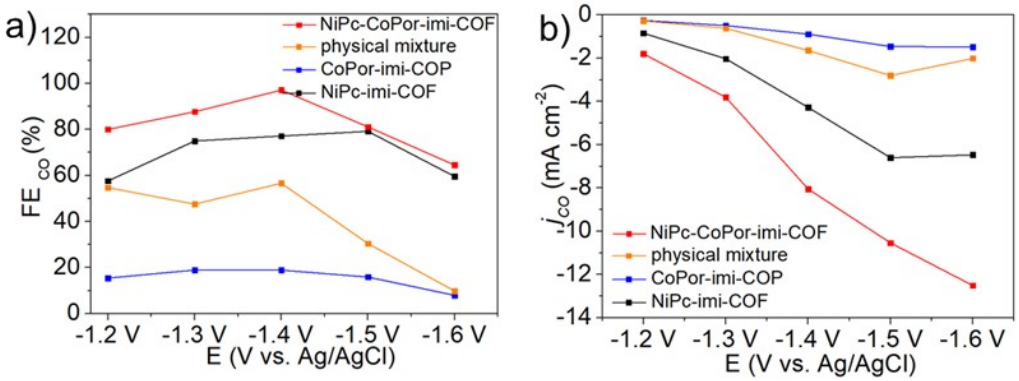

Fig. S21. FE_{CO} a) and j_{CO} b) of NiPc-imi-COF, and CoPor-imi-COP, NiPc-CoPor-imi-COF, and the physical mixture NiPc-imi-COF and CoPor-imi-COP (1:1).

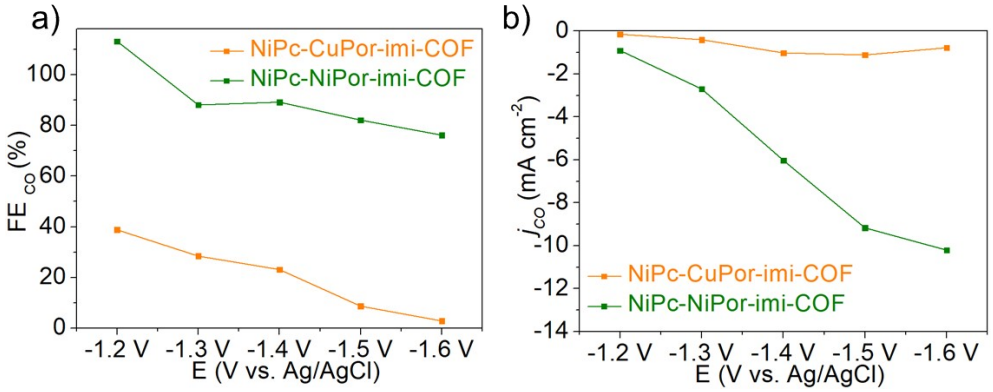

Fig. S22. FE_{CO} a) and j_{CO} b) of NiPc-CuPor-imi-COF and NiPc-NiPor-imi-COF.

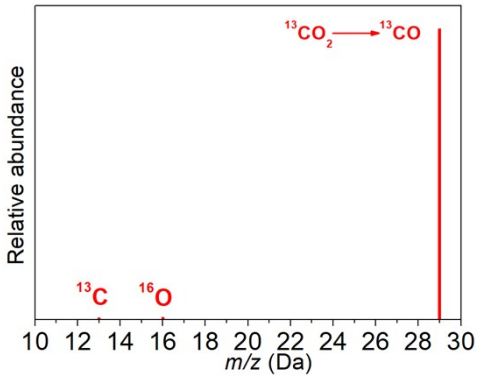

Fig S23. The mass spectra of **NiPc-CoPor-imi-COF** of ^{13}CO recorded under $^{13}CO_2$ atmosphere.

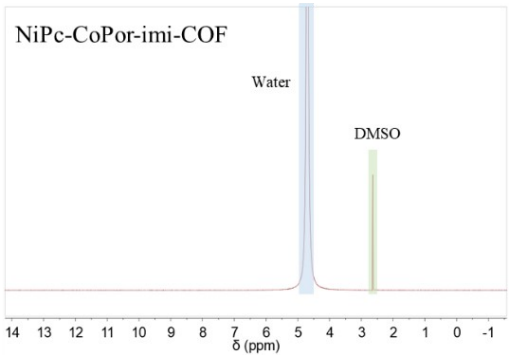

Fig. S24. ^{1}H NMR spectroscopy of the reaction mixture of **NiPc-CoPor-imi-COF** after catalysis, DMSO was added as internal standard.

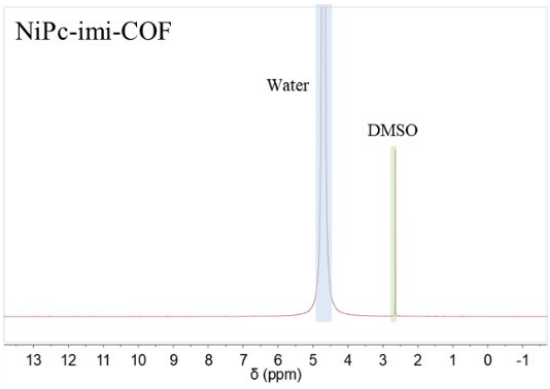

Fig. S25. ^{1}H NMR spectroscopy of the reaction mixture of **NiPc-imi-COF** after catalysis, DMSO was added as internal standard.

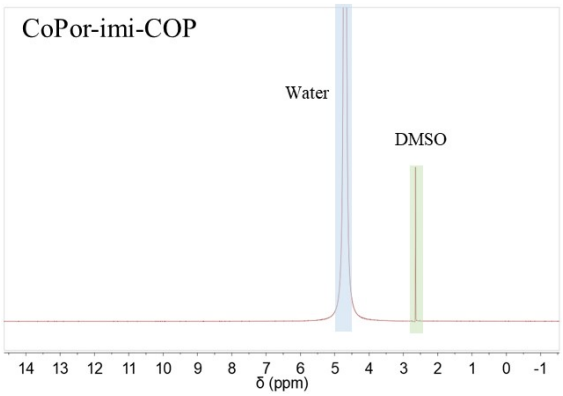

Fig. S26. ^{1}H NMR spectroscopy of the reaction mixture of **CoPor-imi-COP** after catalysis, DMSO was added as internal standard.

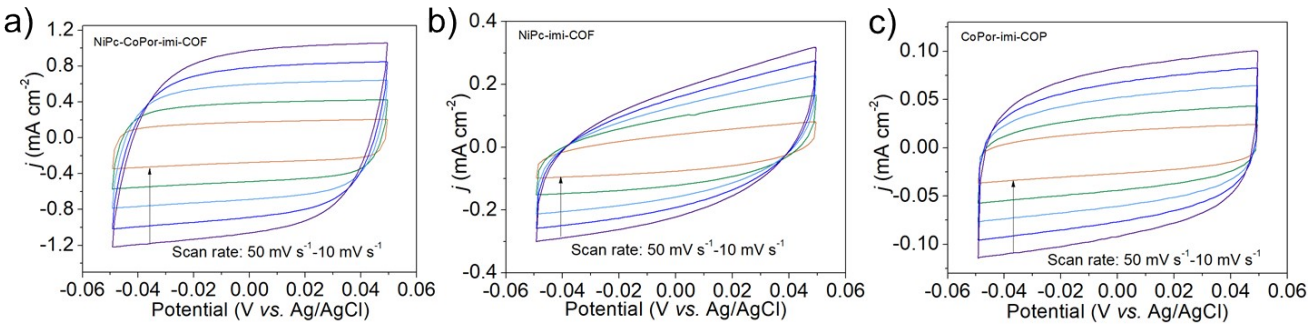

Fig. S27. Cyclic voltammogram (CV) curves in the region from -0.05 to 0.05 V vs. Ag/AgCl at various scan rates (from 10 to 50 mV s^{-1}) and Linear fittings of the current density differences (Δj) with the scan rates to determine the double layer capacitance (C_{dl}) for a, b) NiPc-CoPor-imi-COF, c, d) NiPc-imi-COF, and e, f) CoPor-imi-COP.[8]

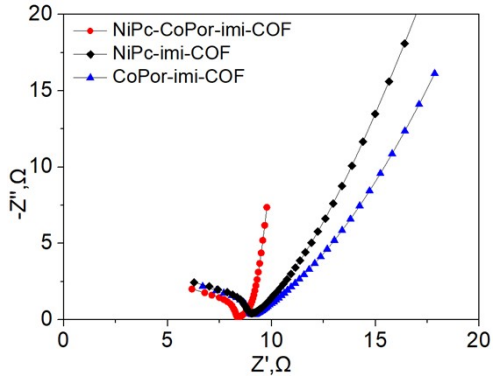

Fig. S28. Electrochemical impedance spectroscopy (EIS) EIS spectra of NiPc-CoPor-imi-COF, NiPc-imi-COF, and CoPor-imi-COP.

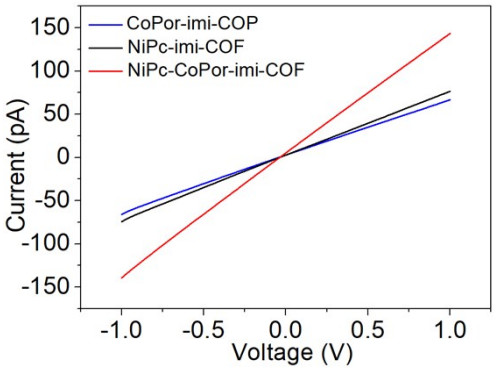

Fig. S29. Electrical measurement of CoPor-imi-COP, NiPc-imi-COF, and NiPc-CoPor-imi-COF were performed using two-electrode in air at a constant temperature of 298 K in the absence of light.

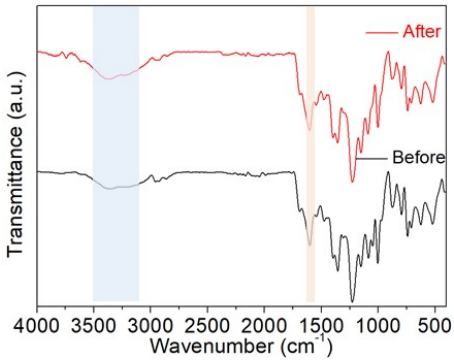

Fig S30. FT-IR spectra of NiPc-CoPor-imi-COF before and after catalysis.

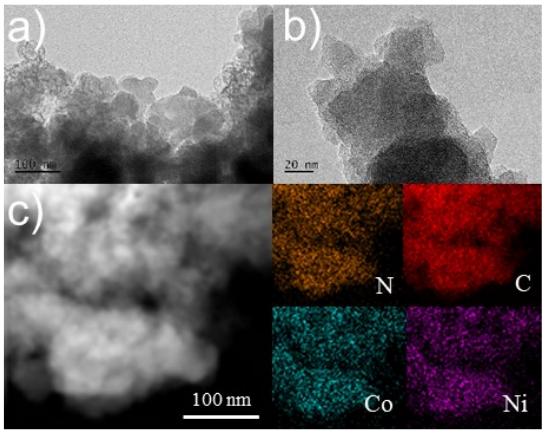

Fig S31. Post characterizations of NiPc-CoPor-imi-COF after the long-term stability test. (a) (b) (c) STEM image of NiPc-CoPor-imi-COF with the corresponding elemental EDS mapping of C, N, Ni and Co, respectively.

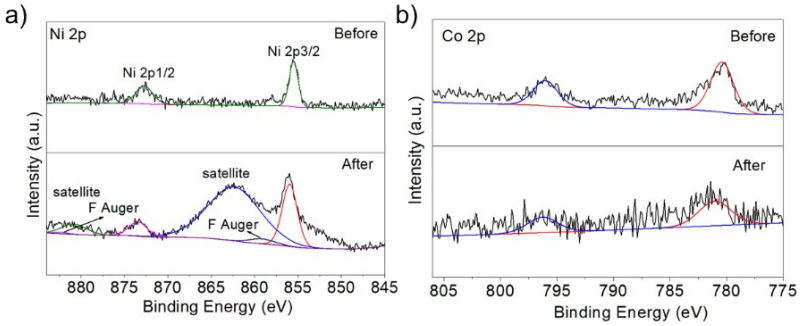

Fig. S32. High-resolution a) Ni 2p and b) Co 2p XPS spectra of NiPc-CoPor-imi-COF before and after CO_2RR testing.

As shown in Fig. S15d, due to the addition of conductive carbon and adhesive Nafion during the preparation of electrode sheets, new peaks appeared in High-resolution Ni 2p XPS spectra of NiPc-CoPor-imi-COF after CO_2RR testing, which have also appeared in previous literature.[9] Specifically, it can be classified as the satellite peak of Ni and the Auger peak of F.[10,11]

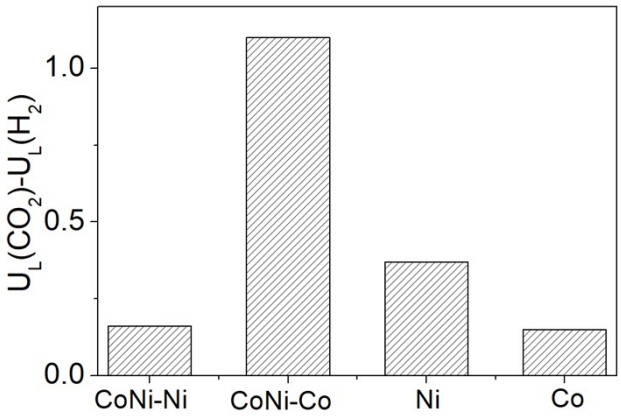

Fig S33. The difference in the limiting potentials for CO_2RR and HER.

3. Supporting Tables

Table S1. EA and ICP-MS analysis results of COFs

Sample	C	N	H	Ni	Co
NiPc-CoPor-imi-COF (Found)	56.33	17.14	4.00	2.96	2.59
NiPc-CoPor-imi-COF (Calculated)	68.77	20.05	2.58	4.23	4.23
NiPc-imi-COF (Found)	57.03	16.51	4.19	4.49	\
NiPc-imi-COF (Calculated)	65.45	25.45	2.27	6.70	
CoPor-imi-COP (Found)	64.03	13.39	4.52	\	4.78
CoPor-imi-COP (Calculated)	73.47	17.14	3.27	\	6.02
8NH_2-NiPc (Found)	\	\	\	7.18	\
8NH_2-NiPc (Calculated)	\	\	\	8.53	\
4CHO-CoPor (Found)	\	\	\	\	7.12
4CHO-CoPor (Calculated)	\	\	\	\	7.53

Table S2. The CO_2 uptakes results normalized byof BET surface areas

	NiPc-imi-COF	**CoPor-imi-COF**	**NiPc-CoPor-imi-COF**
SA_{BET} (cm^2/g)	129.9	532.1	440.9
CO_2 adsorption (cm^3/g)	14.6	31.3	22.6
CO_2 adsorption of SA_{BET} normalized (cm^3/cm^2)	0.112	0.059	0.051
Mass percentage of nitrogen of benzimidazole in the material	0.127	0.114	0.080

Table S3. EXAFS fitting parameters at the Ni K–edge for various samples

Sample	Shell	*CN*[a]	*R*(Å)[b]	σ^2(Å^2)[c]	ΔE_0(eV)[d]	*R* factor
Ni foil	Ni-Ni	12*	2.48±0.01	0.0062±0.0002	5.9±0.4	0.0016
NiPc	Ni-N	4.0±0.6	1.88±0.02	0.0023±0.0015	7.1±1.9	0.0193
Ni sites	**Ni-N**	**4.0±0.7**	**1.88±0.02**	**0.0027±0.0018**	**6.7±2.2**	**0.0173**

[a]*CN*, coordination number; [b]*R*, distance between absorber and backscatter atoms; [c]σ^2, Debye-Waller factor to account for both thermal and structural disorders; [d]ΔE_0, inner potential correction; *R* factor indicates the goodness of the fit. S_0^2 was fixed to 0.81, according to the experimental EXAFS fit of Ni foil by fixing CN as the known crystallographic value. A reasonable range of EXAFS fitting parameters: $0.700 < S_0^2 < 1.000$; $CN > 0$; $\sigma^2 > 0$ Å^2; $|\Delta E_0| < 10$ eV; *R* factor < 0.02.

Table S4. EXAFS fitting parameters at the Co K–edge for various samples

Sample	Shell	*CN*[a]	*R*(Å)[b]	σ^2(Å^2)[c]	ΔE_0(eV)[d]	*R* factor
Co foil	Co-Co	12*	2.49±0.01	0.0063±0.0002	7.2±0.3	0.0010
CoO	Co-O	6.0±1.0	2.11±0.03	0.0072±0.0022	8.9±1.6	0.0098
	Co-O-Co	12.3±1.9	3.01±0.01	0.0088±0.0009	9.7±1.1	
Co sites	**Co-N**	**4.1±0.6**	**1.91±0.02**	**0.0016±0.0012**	**8.0±1.5**	**0.0136**

[a]*CN*, coordination number; [b]*R*, distance between absorber and backscatter atoms; [c]σ^2, Debye-Waller factor to account for both thermal and structural disorders; [d]ΔE_0, inner potential correction; *R* factor indicates the goodness of the fit. S_0^2 was fixed to 0.71, according to the experimental EXAFS fit of Co foil by fixing CN as the known crystallographic value. A reasonable range of EXAFS fitting parameters: $0.700 < S_0^2 < 1.000$; $CN > 0$; $\sigma^2 > 0$ Å^2; $|\Delta E_0| < 10$ eV; *R* factor < 0.02.

Table S5 Summary of TOF at -1.4 V vs. Ag/AgCl (s^{-1}).

Catalyst	TOF_{ICP}
NiPc-CoPor-imi-COF	0.04433
NiPc-imi-COF	0.02911
CoPor-imi-COP	0.0057

Table S6. Conductivity of CoPor-imi-COP, NiPc-imi-COF, and NiPc-CoPor-imi-COF measured by two probe method.

sample	CoPor-imi-COP	NiPc-imi-COF	NiPc-CoPor-imi-COF
σ (S m^{-1})	1.31 ×10^{-6}	1.49 ×10^{-6}	2.81 ×10^{-6}

Table S7. Ni and Co content analysis results of the electrolyte for NiPc-CoPor-imi-COF after CO_2RR testing.

sample	Ni [mg/L]	Co [mg/L]
NiPc-CoPor-imi-COF	no detected	no detected

Table S8. Comparison of CO Faradaic efficiency of various catalysts for CO_2 electroreduction. (Purple: Porphyrin COFs, blue: phthalocyanine COFs, pink: Bipyridyl COFs, brown: Amorphous porous materials).

Catalyst	E (V vs. RHE)	CO		TOF (s^{-1})	Ref.
		FE%	$\|J\|$ (mA/cm^{-2})		
NiPc-CoPor-imi-COF	−0.77	97.1	8.0	0.044	This work
COF-366-Co	−0.67	90	1.8	0.027	12
COF-367-Co	−0.67	91	3.3	0.046	
COF-Re_Co	−1.1	18(2)	-	-	13
COF-F-Co	−0.67	87	-	-	14
COF-300-AR on Ag film	−0.85	80	1.8	-	15
NiSAs/PTF	−0.8	98	17	3.74 (-1.2 V)	16
Co-TTCOF NSs	−0.8	99.7	-	-	17
Co-TTCOF	−0.7	91.3	~2	1.25	
Ni-TTCOF	−0.9	20.9	~2.2	-	
TTF-Por (Co)-COF	−0.7	95	6.88 (-0.9 V)	0.12	10
TT-Por(Co)-COF	−0.6	91.4	7.28 (-0.7 V)	0.13 (−0.7 V)	18
CoPor-N3	−0.50	96	19.5	0.153	2
TPPDA-CoPor-COF	−0.9	90	15.3	1.4	19
3D-Por(Co/H)-COF	−0.60	92.4	15.5 (-1.1 V)	1.28	20
TPE-CoPor-COF	−0.7	95	9.3	0.72	21
TAPP(Co)-B18C6-COF	−0.7	93.3	9.45(-1.0 V)	0.19	22
NiPc-COF	−0.9	99.1	35 (-1.1 V)	1.05	23
CoPc-PI-COF-1	−0.9	95	21.2	4.9	24
CoPc-PI-COF-3	−0.9	96	31.7	0.6	25
NiPc-TFPN COF	−0.9	99.8	14.1	0.14	26
CoPc-TFPN COF		96	10.6	0.10	
CuPcF8-CoPc-COF	−0.7	91	15.2	1.25	27
CuPcF8-CoNPc-COF	−0.62	97	16.5	2.87	
CoPc-2H_2Por COF	−0.55	95	7.7	~0.1	28
CoPc-H_2Por COF	−0.6	94	-	~0.07	
COF-2,2′-bpy-Re 29.38 wt% Re	–2.8 V vs. Fc+/0	81	-10.7	-	29
COFbpyMn|NT	–1.34 V vs. SCE	40	1.4(1h)	~0.16	30
COF@CoPor	−0.6	94.3	12.5 (-1.0 V)	1.27	31
TTF-1	η = 0.56 V	~ 82	1.2		32

Co-CTF	−0.7	85	1	-	[33]
Ni-CTF	−0.9	95	1.7	-	
Cu-CTF	−1.0	7	0.2	-	
NiPor-CTF	−0.9	97	52.9	0.47	[34]
COPs (COP-SA)	−0.65	96.5	9.74	46	[35]
CoPc-1	−0.66	94	-	0.29	[36]

Supporting References

1 X.-Y. Dong, Y.-N. Si, Q.-Y. Wang, S. Wang and S.-Q. Zang, *Adv. Mater.*, 2021, **33**, 2101568.
2 T. Wang, L. Guo, H. Pei, S. Chen, R. Li, J. Zhang and T. Peng, *Small*, 2021, **17**, 2102957.
3 J. P. Perdew, K. Burke and M. Ernzerhof, *Phys Rev Lett*, 1996, **77**, 3865-3868.
4 B. Hammer, L. B. Hansen and J. K. Nørskov, *Physical Review B*, 1999, **59**, 7413-7421.
5 P. E. Blöchl, *Physical Review B*, 1994, **50**, 17953-17979.
6 G. Kresse and D. Joubert, *Physical Review B*, 1999, **59**, 1758-1775.
7 H. J. Monkhorst and J. D. Pack, *Physical Review B*, 1976, **13**, 5188-5192.
8 B. Chen, B. Li, Z. Tian, W. Liu, W. Liu, W. Sun, K. Wang, L. Chen and J. Jiang, *Adv. Energy Mater.*, 2021, **11**, 2102152.
9 M. D. Zhang, D. H. Si, J. D. Yi, S. S. Zhao, Y. B. Huang and R. Cao, *Small*, 2020, **16**, e2005254.
10 Q. Wu, R.-K. Xie, M.-J. Mao, G.-L. Chai, J.-D. Yi, S.-S. Zhao, Y.-B. Huang and R. Cao, *ACS Energy Lett.*, 2020, **5**, 1005-1012.
11 F. Wang, G. Wang, P. Deng, Y. Chen, J. Li, D. Wu, Z. Wang, C. Wang, Y. Hua and X. Tian, *Small*, 2023, 10.1002/smll.202301128.
12 S. Lin, C. S. Diercks, Y.-B. Zhang, N. Kornienko, E. M. Nichols, Y. Zhao, A. R. Paris, D. Kim, P. Yang and O. M. Yaghi, *Science*, 2015, **349**, 1208-1213.
13 E. M. Johnson, R. Haiges and S. C. Marinescu, *ACS Appl. Mater. Interfaces*, 2018, **10**, 37919-37927.
14 C. S. Diercks, S. Lin, N. Komienko, E. A. Kapustin, E. M. Nichols, C. Zhu, Y. Zhao, C. J. Chang and O. M. Yaghi, *J. Am. Chem. Soc.*, 2018, **140**, 1116-1122.
15 H. Liu, J. Chu, Z. Yin, X. Cai, L. Zhuang and H. Deng, *Chem*, 2018, **4**, 1696-1709.
16 Y. Hou, Y.-B. Huang, Y.-L. Liang, G.-L. Chai, J.-D. Yi, T. Zhang, K.-T. Zang, J. Luo, R. Xu, H. Lin, S.-Y. Zhang, H.-M. Wang and R. Cao, *CCS Chem.*, 2019, **1**, 384-395.
17 H. J. Zhu, M. Lu, Y. R. Wang, S. J. Yao, M. Zhang, Y. H. Kan, J. Liu, Y. Chen, S. L. Li and Y. Q. Lan, *Nat. Commun.*, 2020, **11**, 497.
18 Q. Wu, M.-J. Mao, Q.-J. Wu, J. Liang, Y.-B. Huang and R. Cao, *Small*, 2021, **17**, 2004933.
19 L. Gong, B. Chen, Y. Gao, B. Yu, Y. Wang, B. Han, C. Lin, Y. Bian, D. Qi and J. Jiang, *Inorg. Chem. Front.*, 2022, **9**, 3217-3223.
20 S.-Y. Chi, Q. Chen, S.-S. Zhao, D.-H. Si, Q.-J. Wu, Y.-B. Huang and R. Cao, *J. Mater. Chem.A*, 2022, **10**, 4653-4659.
21 L. Gong, Y. Gao, Y. Wang, B. Chen, B. Yu, W. Liu, B. Han, C. Lin, Y. Bian, D. Qi and J. Jiang, *Catal. Sci. Technol*, 2022, **12**, 6566-6571.
22 S. An, C. Lu, Q. Xu, C. Lian, C. Peng, J. Hu, X. Zhuang and H. Liu, *ACS Energy Lett.*, 2021, **6**, 3496-3502.
23 M.-D. Zhang, D.-H. Si, J.-D. Yi, S.-S. Zhao, Y.-B. Huang and R. Cao, *Small*, 2020, **16**, 2005254.
24 B. Han, X. Ding, B. Yu, H. Wu, W. Zhou, W. Liu, C. Wei, B. Chen, D. Qi, H. Wang, K. Wang, Y. Chen, B. Chen and J. Jiang, *J. Am. Chem. Soc.*, 2021, **143**, 7104-7113.
25 B. Han, Y. Jin, B. Chen, W. Zhou, B. Yu, C. Wei, H. Wang, K. Wang, Y. Chen, B. Chen and J. Jiang, *Angew. Chem. Int. Ed.*, 2022, **61**, e202114244.
26 M. Lu, M. Zhang, C.-G. Liu, J. Liu, L.-J. Shang, M. Wang, J.-N. Chang, S.-L. Li and Y.-Q. Lan, *Angew. Chem. Int. Ed.*, 2021, **60**, 4864-4871.
27 Y. Yue, P. Cai, K. Xu, H. Li, H. Chen, H.-C. Zhou and N. Huang, *Journal of the American Chemical Society*, 2021, **143**, 18052–18060.
28 J. Yuan, S. Chen, Y. Zhang, R. Li, J. Zhang and T. Peng, *Adv. Mater.*, 2022, **34**, e2203139.
29 D. A. Popov, J. M. Luna, N. M. Orchanian, R. Haiges, C. A. Downes and S. C. Marinescu, *Dalton Transactions*, 2018, **47**, 17450-17460.
30 G. C. Dubed Bandomo, S. S. Mondal, F. Franco, A. Bucci, V. Martin-Diaconescu, M. A. Ortuño, P. H. van Langevelde, A. Shafir, N. López and J. Lloret-Fillol, *ACS Catal.*, 2021, **11**, 7210-7222.
31 L. Zhai, S. Yang, C. Lu, C.-X. Cui, Q. Xu, J. Liu, X. Yang, X. Meng, S. Lu, X. Zhuang, G. Zeng and Z. Jiang, *Small*, **18**, 2200736.
32 X. Zhu, C. Tian, H. Wu, Y. He, L. He, H. Wang, X. Zhuang, H. Liu, C. Xia and S. Dai, *ACS applied materials & interfaces*, 2018, **10**, 43588-43594.
33 P. Su, K. Iwase, T. Harada, K. Kamiya and S. Nakanishi, *Chem. Sci.*, 2018, **9**, 3941-3947.
34 C. Lu, J. Yang, S. Wei, S. Bi, Y. Xia, M. Chen, Y. Hou, M. Qiu, C. Yuan, Y. Su, F. Zhang, H. Liang and X. Zhuang, *Adv. Funct. Mater.*, 2019, **29**, 1806884.
35 Y. Song, J.-J. Zhang, Z. Zhu, X. Chen, L. Huang, J. Su, Z. Xu, T. H. Ly, C.-S. Lee, B. I. Yakobson, B. Z. Tang and R. Ye, *Appl. Catal. B*, 2021, **284**, 119750.
36 J. Luangchaiyaporn, D. Wielend, D. Solonenko, H. Seelajaroen, J. Gasiorowski, M. Monecke, G. Salvan, D. R. T. Zahn, N. S. Sariciftci and P. Thamyongkit, *Electrochim. Acta*, 2021, **367**, 137506.